Supplementary Materials for

An NIR-Fluorophore-Based Theranostic for Selective Initiation of Tumor Pyroptosis Induced Immunotherapy

Kewei Wang, Xuan Xiao, Maolin Jiang, Jisi Li, Jielian Zhou and Youyong Yuan*

*Corresponding author. Email: yuanyy@scut.edu.cn

This PDF file includes:

Figs. S1 to S32
Movie S1

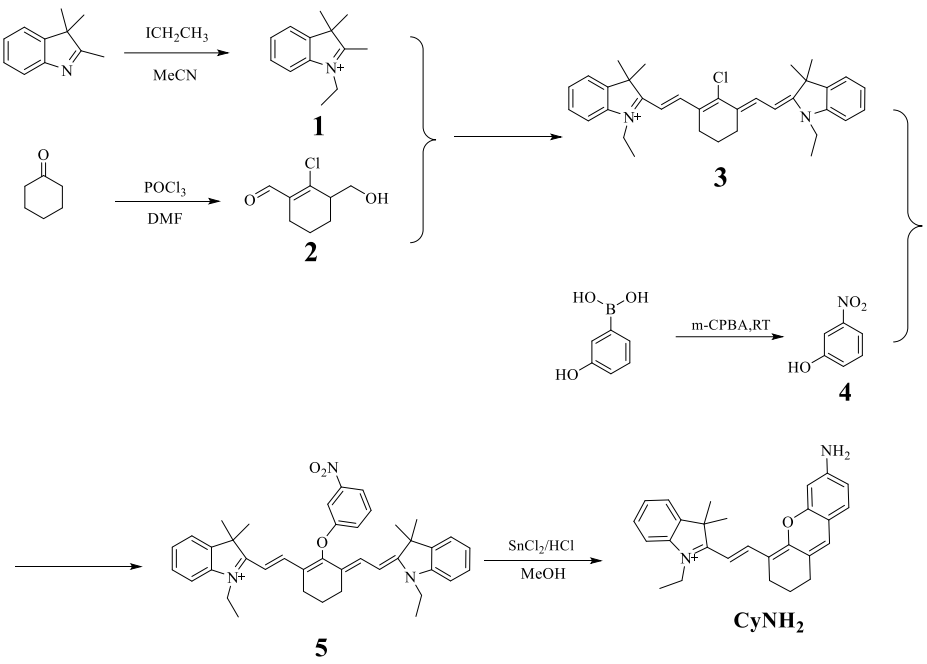

Scheme S1. Synthetic procedures of $CyNH_2$. DMF: *N*,*N*-dimethylformamide, m-CPBA: m-chloroperoxybenzoic acid, RT: room temperature.

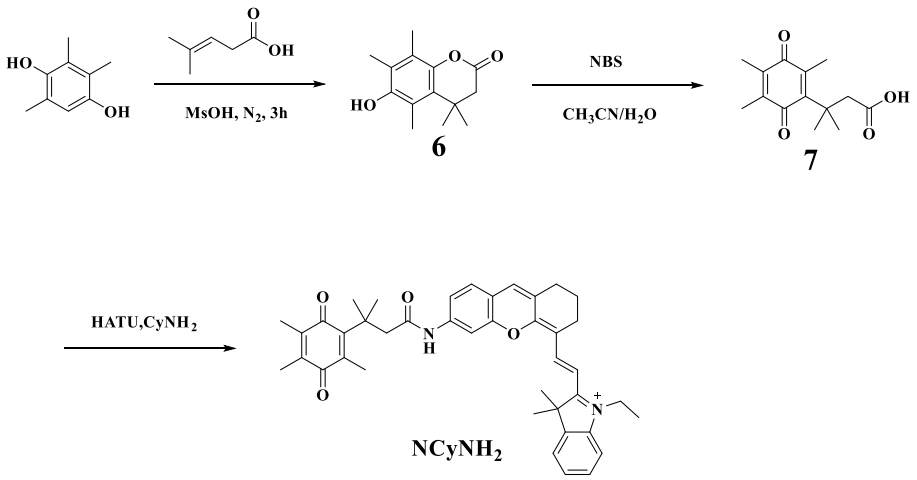

Scheme S2. Synthetic procedures of $NCyNH_2$. NBS: *N*-bromosuccinimide, HATU: 2-(7-azabenzotriazole)-*N*,*N*,*N'*,*N'*-tetramethylurea hexafluorophosphate.

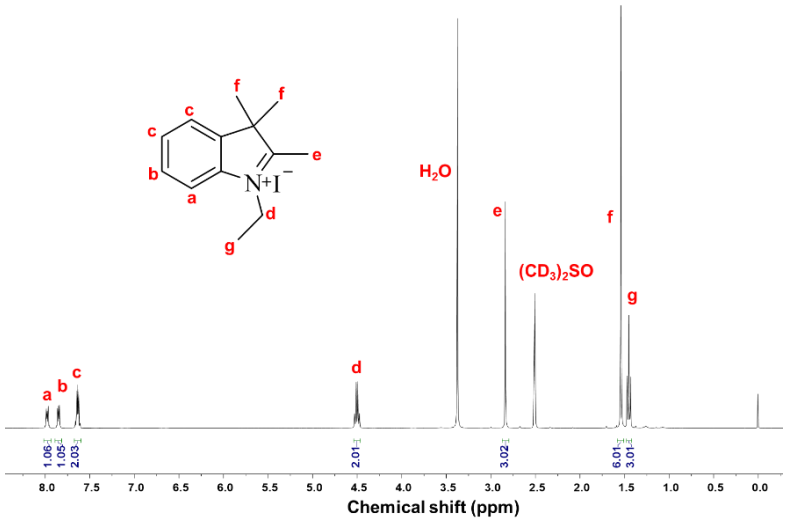

Fig. S1. ^{1}H NMR spectrum of compound **1** in DMSO-d_6.

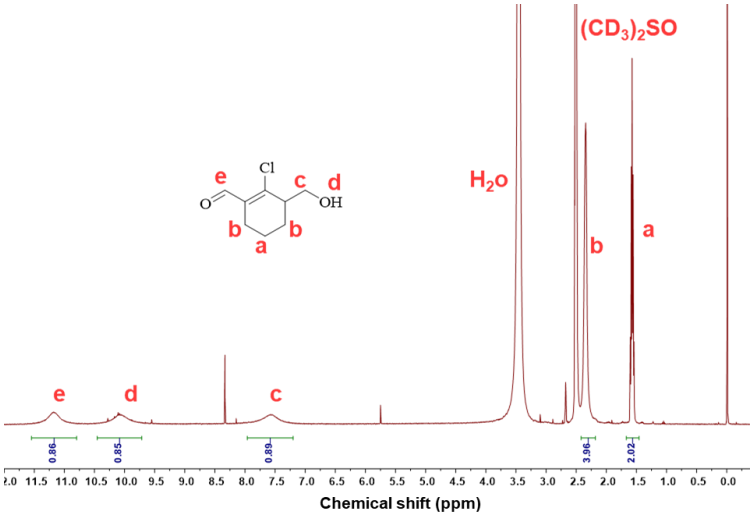

Fig. S2. ^{1}H NMR spectrum of compound **2** in DMSO-d_6.

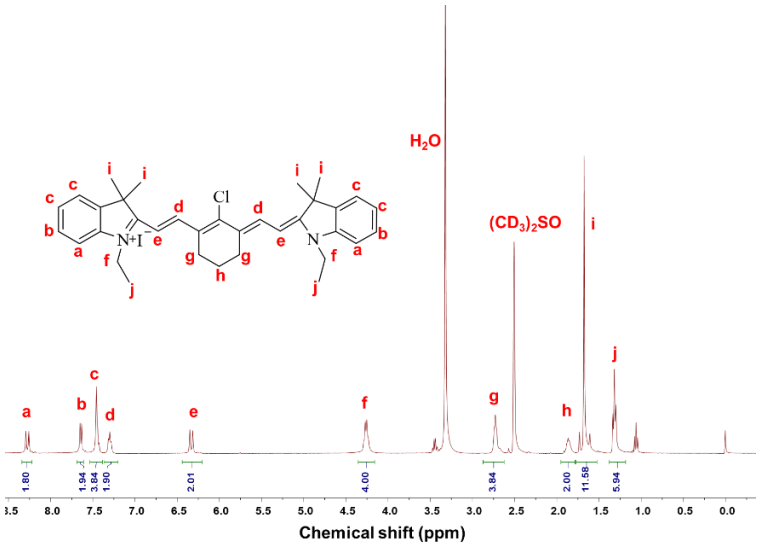

Fig. S3. ^{1}H NMR spectrum of compound **3** in DMSO-d_6.

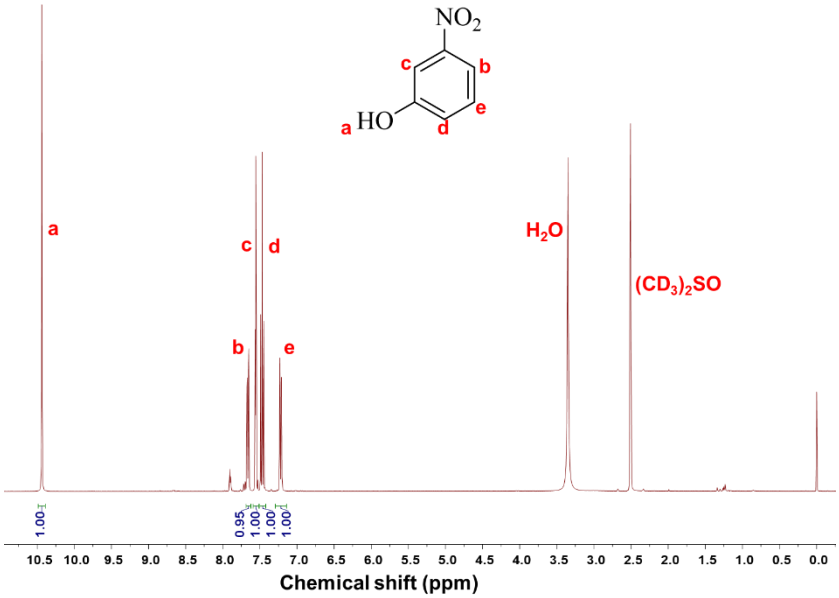

Fig. S4. ^{1}H NMR spectrum of compound **4** in DMSO-d_6.

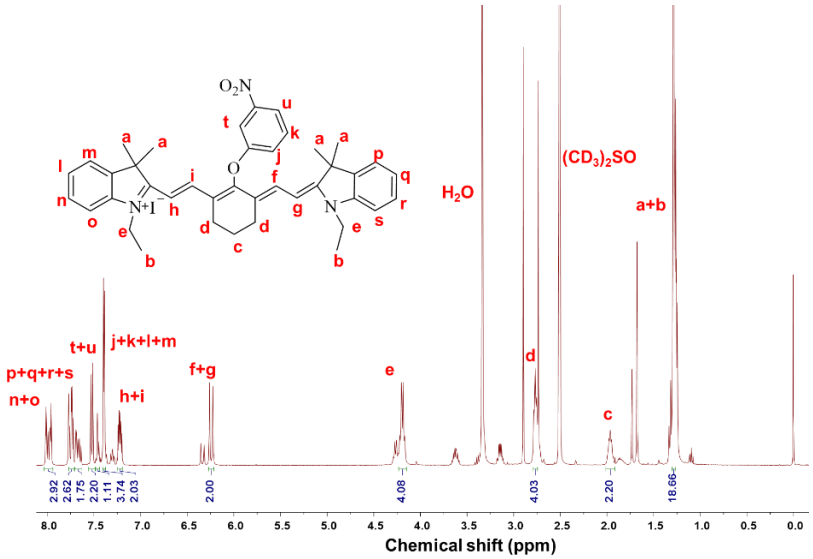

Fig. S5. ^{1}H NMR spectrum of compound **5** in DMSO-d_6.

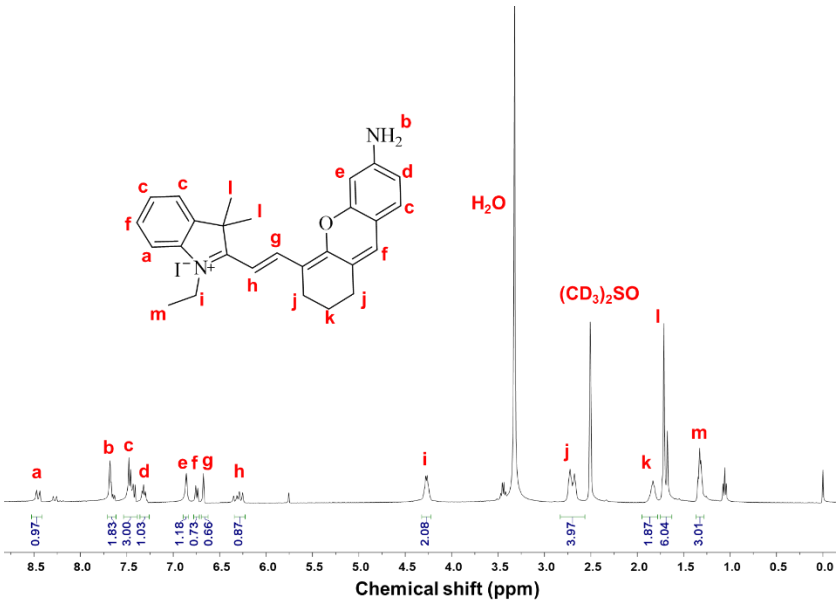

Fig. S6. ^{1}H NMR spectrum of $CyNH_2$ in DMSO-d_6.

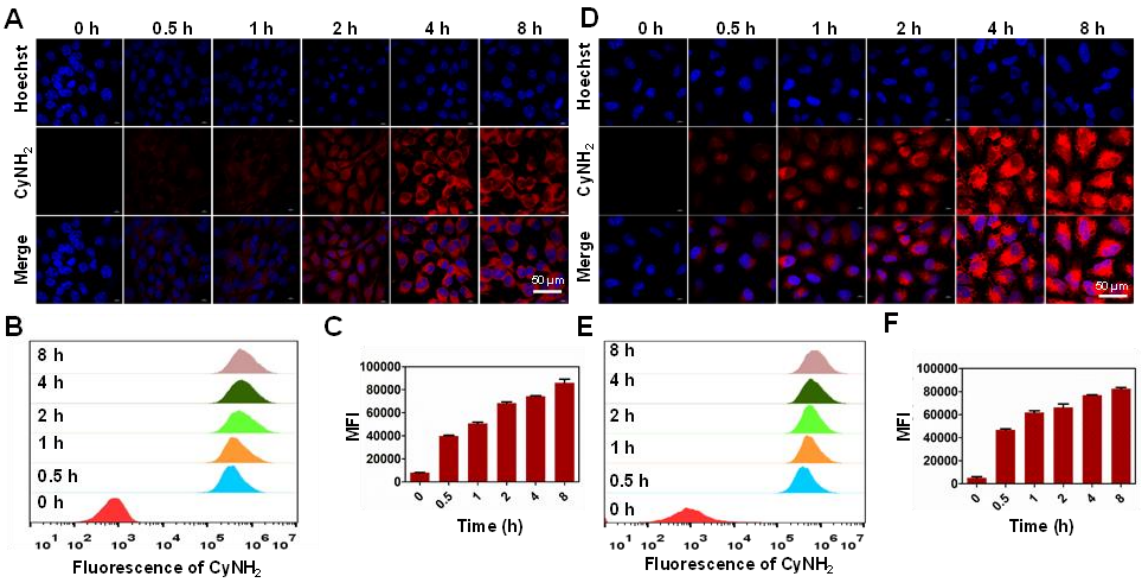

Fig. S7. (A) Confocal images of 4T1 cells incubated with $CyNH_2$ for different time durations. The red fluorescence is from $CyNH_2$. (B, C) Quantitative analysis of the fluorescence intensity of $CyNH_2$ in 4T1 cells by flow cytometry. (D) Confocal images of CT26 cells incubated with $CyNH_2$ for different time durations. The red fluorescence is from $CyNH_2$. (E, F) Quantitative analysis of the fluorescence intensity of $CyNH_2$ in CT26 cells by flow cytometry.

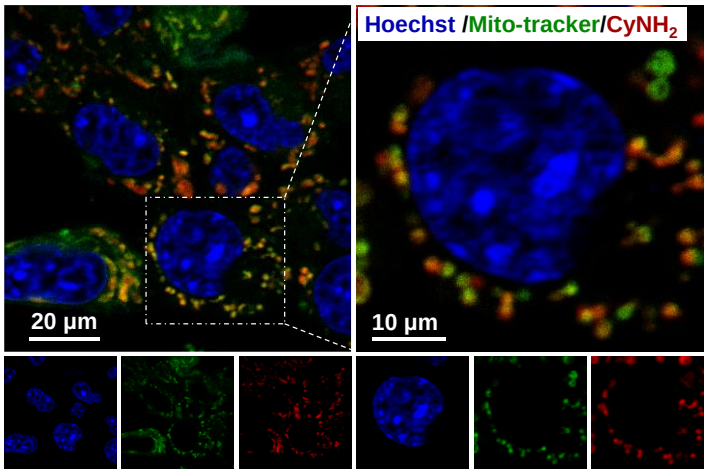

Fig. S8. The intracellular localization of $CyNH_2$ in CT26 cells.

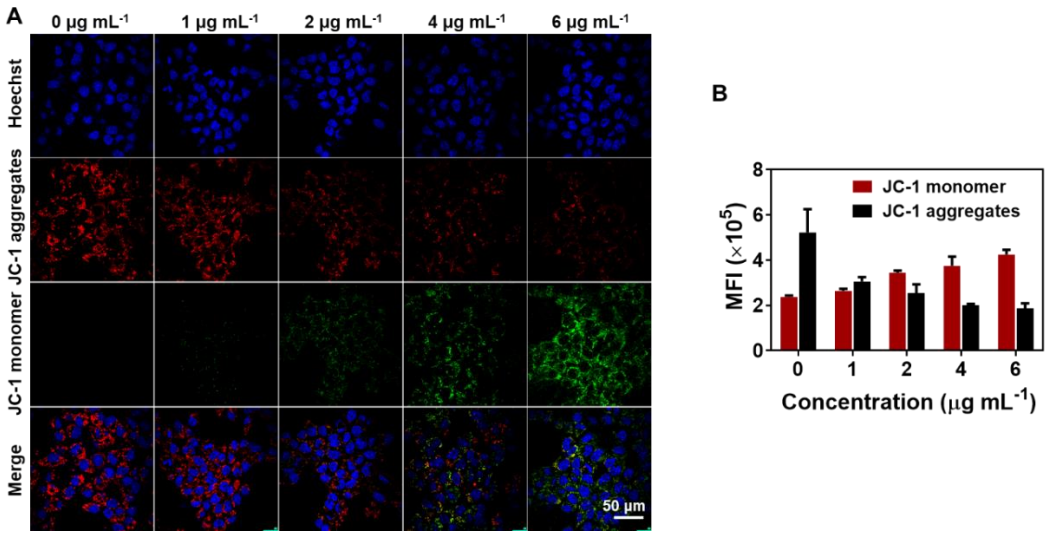

Figure S9. (A) Confocal images showing the measurement of mitochondrial membrane potential using JC-1 in 4T1 cells incubated with different concentrations of $CyNH_2$ for 4 h. (B) The quantitative analysis the fluorescence intensity of JC-1 monomer and JC-1 aggregates in 4T1 cells by flow cytometry upon incubating the cells with different concentrations of $CyNH_2$ for 4 h.

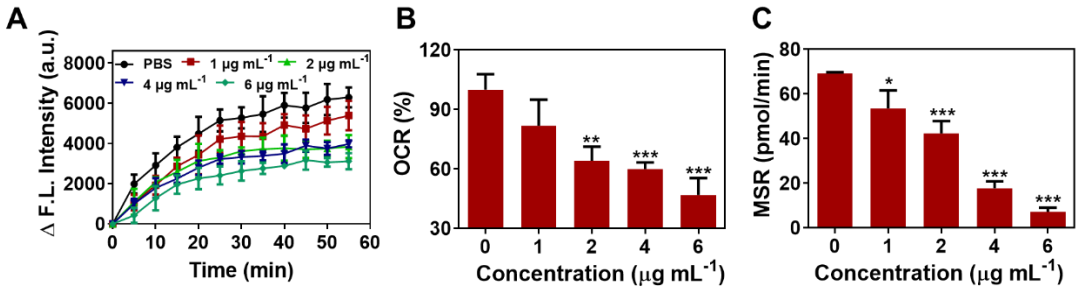

Fig. S10. (A) The fluorescence intensity change of the oxygen sensitive fluorescent probe in 4T1 cells pretreated with different concentrations of $CyNH_2$. (B) The mitochondrial oxygen consumption rate (OCR) after incubation with different concentrations of $CyNH_2$. (C) The mitochondrial respiration rate (MRR) after incubation with different concentrations of $CyNH_2$. Data are presented as the mean ± SD. Statistical analysis was performed using the one-way ANOVA test (ns, nonsignificant. *$P < 0.05$, **$P < 0.01$, and ***$P < 0.001$).

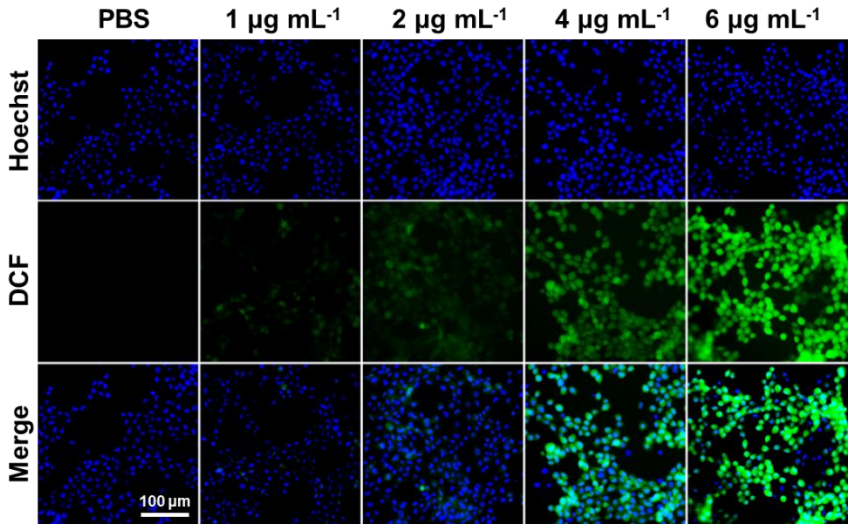

Fig. S11. The ROS level in 4T1 cells treated with different concentrations of $CyNH_2$ using DCFH-DA as indicator. The green fluorescence is from DCF.

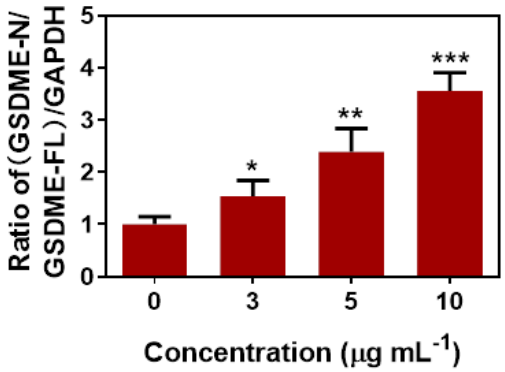

Fig. S12. The ratio of (GSDME-N/GSDME-FL)/GAPDH in 4T1 cells after treatment with different concentrations of $CyNH_2$. Data are presented as the mean ± SD. Statistical analysis was performed using the one-way ANOVA test (ns, nonsignificant. *P < 0.05, **P < 0.01, and ***P < 0.001).

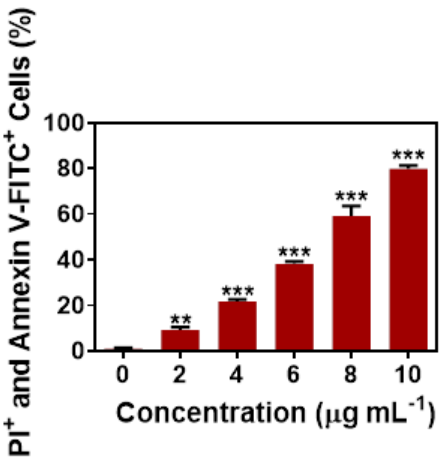

Fig. S13. Absolute quantification of 4T1 cells for apoptosis and necrosis after treatment with different concentrations of $CyNH_2$. Data are presented as the mean ± SD. Statistical analysis was performed using the one-way ANOVA test (ns, nonsignificant. *P < 0.05, **P < 0.01, and ***P < 0.001).

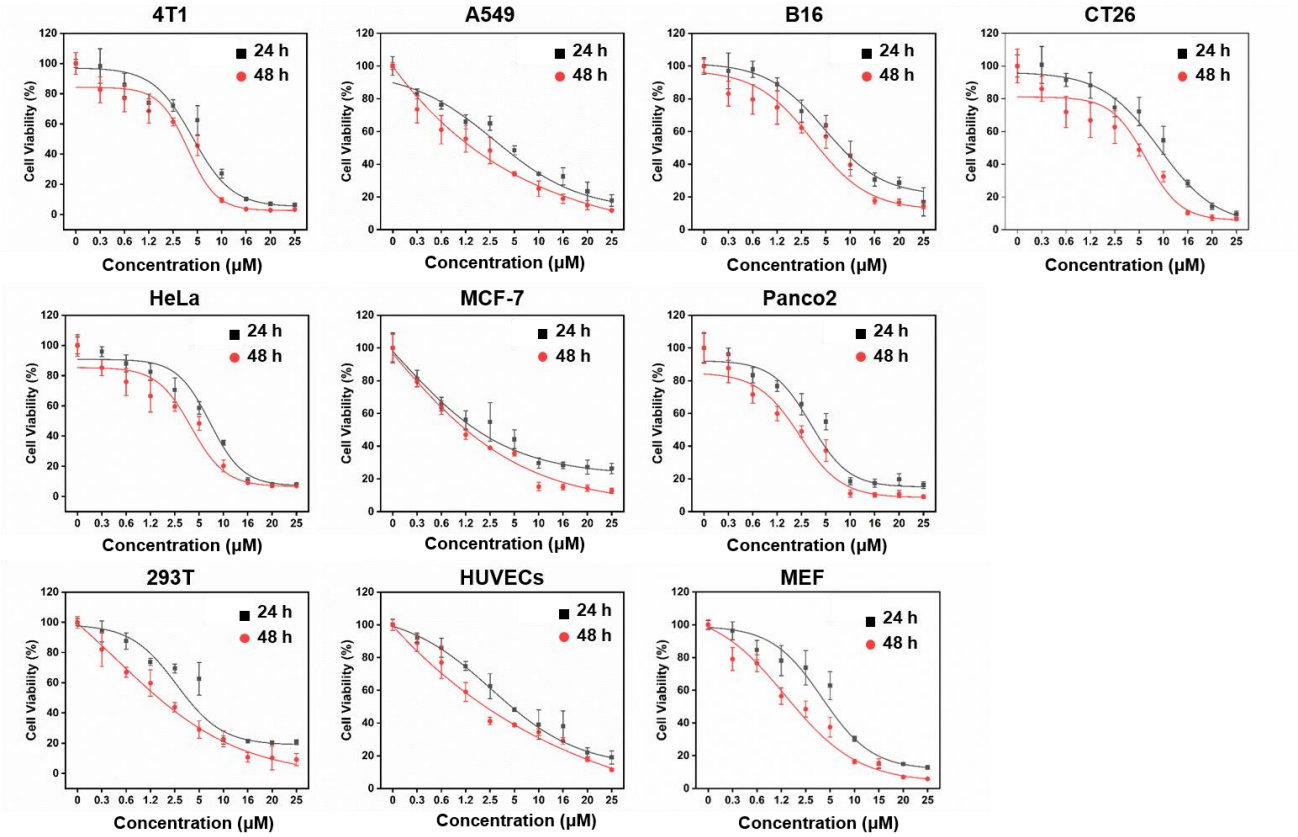

Fig. S14. Cell viability of various cells treated with different concentrations of $CyHN_2$.

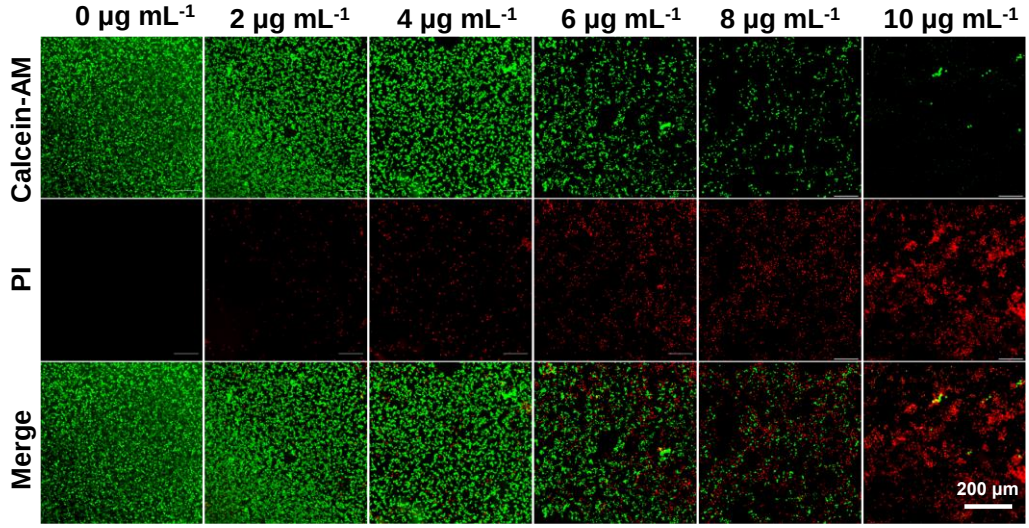

Fig. S15. Live/dead staining of 4T1 cells treated with different concentrations of $CyNH_2$ (green fluorescence represents live cells stained with Calcein-AM and red fluorescence represents dead cells stained with propidium iodide (PI)).

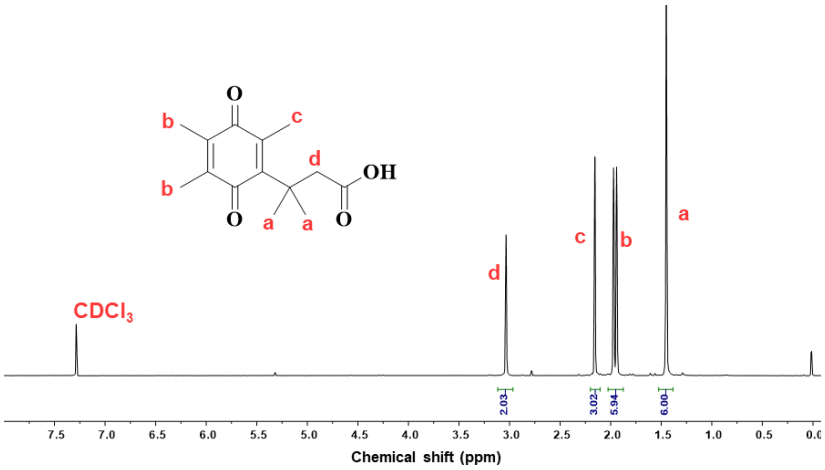

Fig. S16. ^{1}H NMR spectrum of compound **6** in $CDCl_3$.

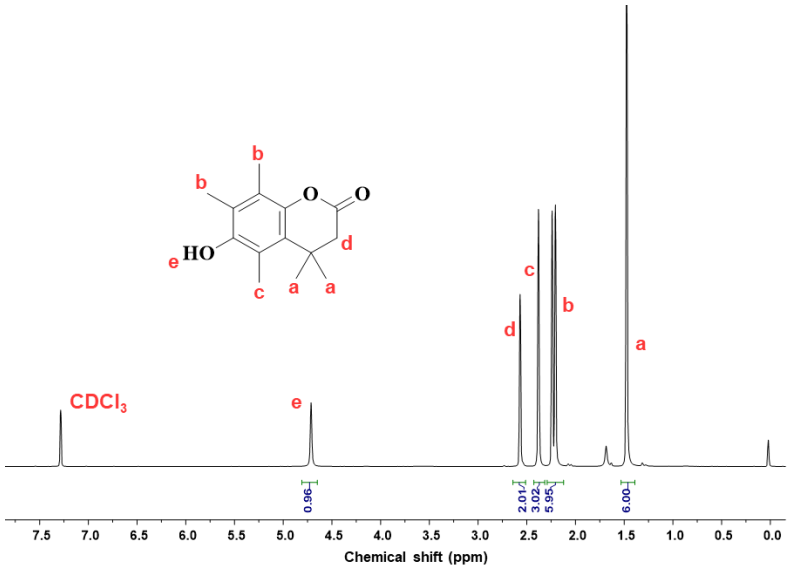

Fig. S17. ^{1}H NMR spectrum of compound **7** in $CDCl_3$.

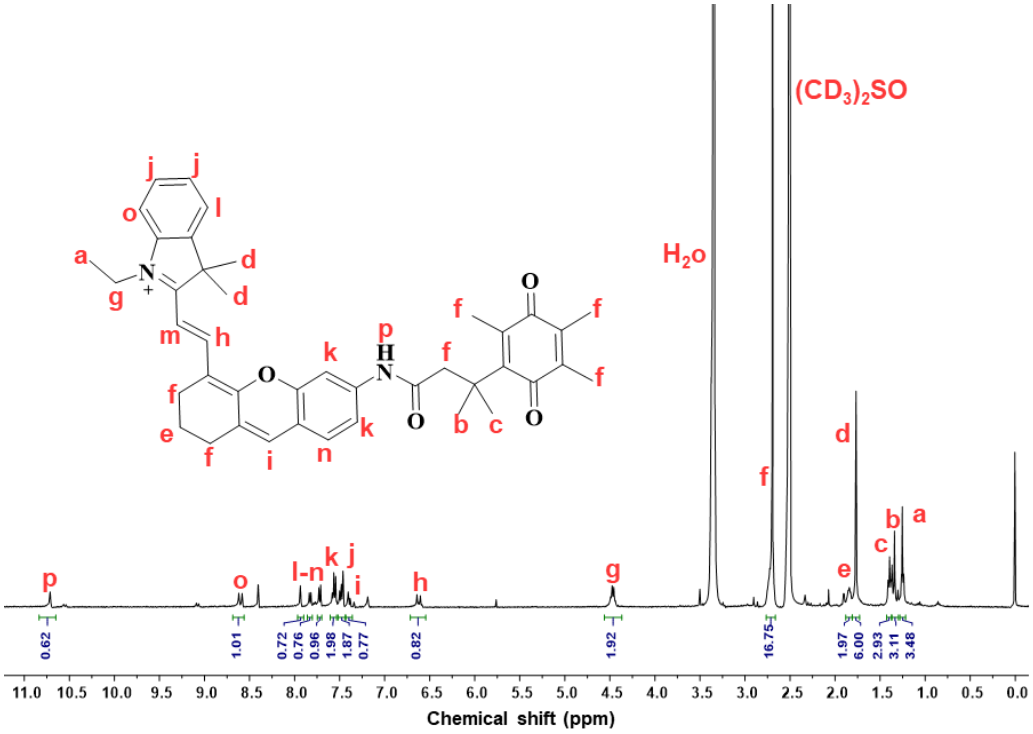

Fig. S18. ^{1}H NMR spectrum of $NCyNH_2$ in DMSO-d_6.

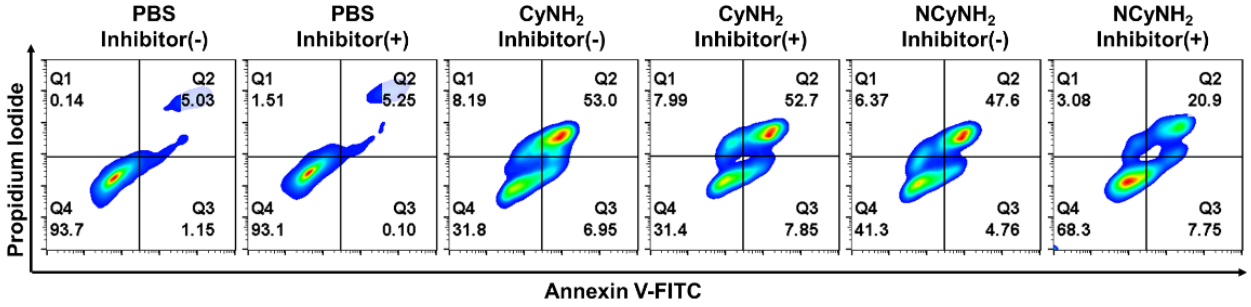

Fig. S19. Flow cytometric analysis of apoptosis and necrosis of 4T1 cells treated with $CyNH_2$ or $NCyNH_2$ (8 μg mL^{-1}) for 8 h in the absence or presence of NQO1 inhibitor (dicoumarol, 50 μM, 1 h pretreatment).

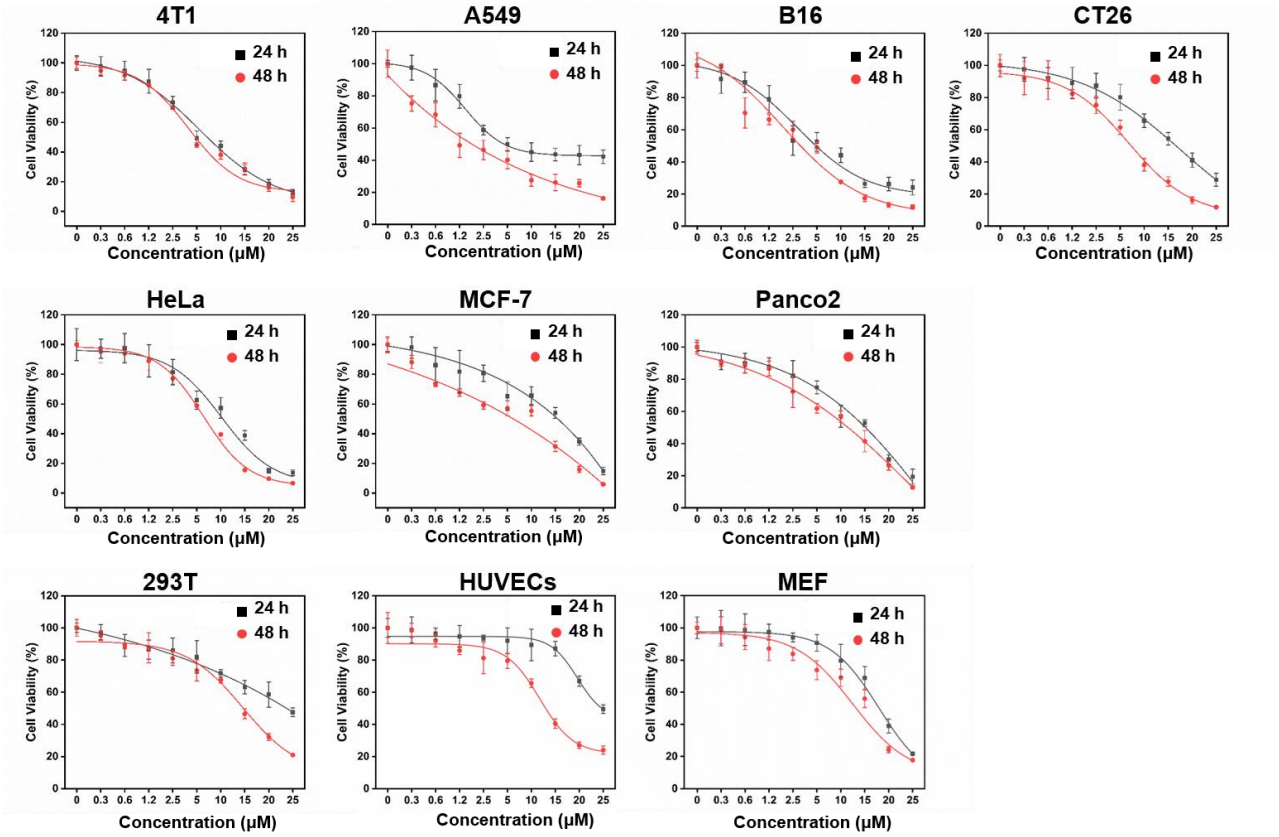

Fig. S20. Cell viability of various cells treated with different concentrations of $NCyHN_2$.

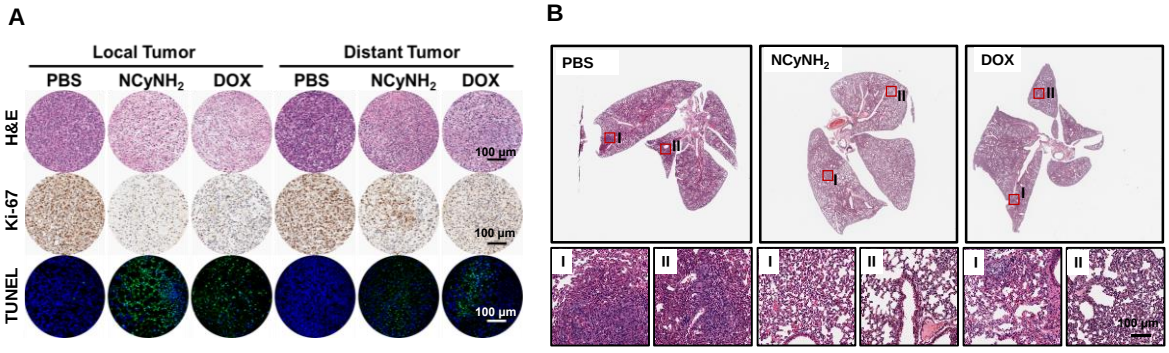

Fig. S21. (A) Representative H&E, Ki-67 and TUNEL staining of bilateral tumors (local and distant) isolated from the 4T1 tumor-bearing mice receiving different treatments. (B) Representative H&E staining of lungs isolated from the 4T1 tumor-bearing mice receiving different treatments.

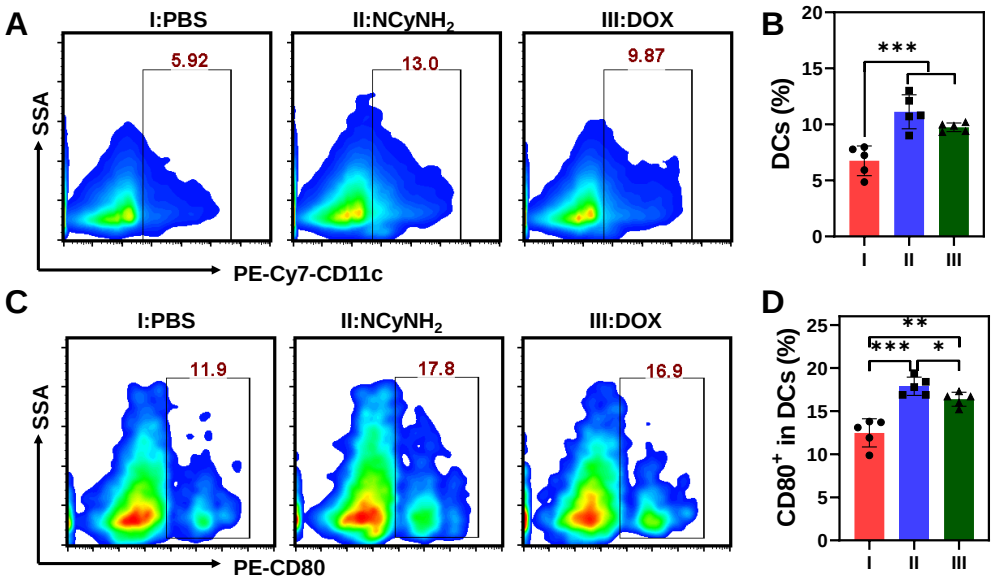

Fig. S22. (A) The representative flow cytometric analysis of DCs ($CD11c^+$ $CD45^+$) in tumor infiltrating leukocytes. (B) The corresponding quantification the percentage of DCs in tumor infiltrating leukocytes. (C) The representative flow cytometric analysis of $CD80^+$ cells in DCs. (D) The corresponding quantification the percentage of $CD80^+$ cells in DCs. Data are presented as the mean ± SD. Statistical analysis was performed using the Student's t test (ns, nonsignificant. **P* < 0.05, ***P* < 0.01, and ****P* < 0.001).

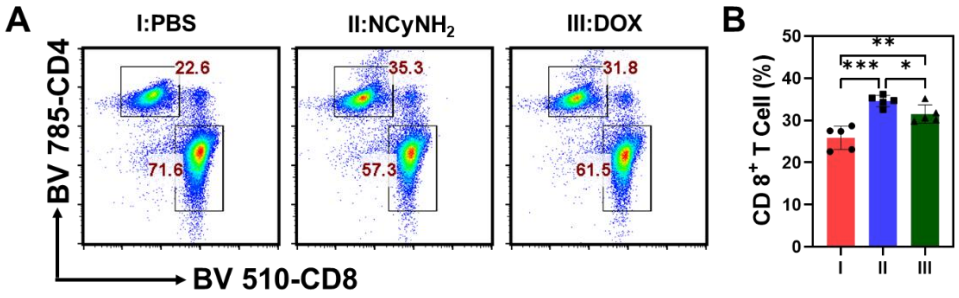

Fig. S23. (A) The representative flow cytometric analysis of $CD8^+$ T cells in the $CD45^+CD3^+$ leukocytes in TDLNs. (B) The corresponding quantification the percentage of $CD8^+$ T cells in the $CD45^+CD3^+$ leukocytes in TDLNs. Data are presented as the mean ± SD. Statistical analysis was performed using the Student's t test (ns, nonsignificant. **P* < 0.05, ***P* < 0.01, and ****P* < 0.001).

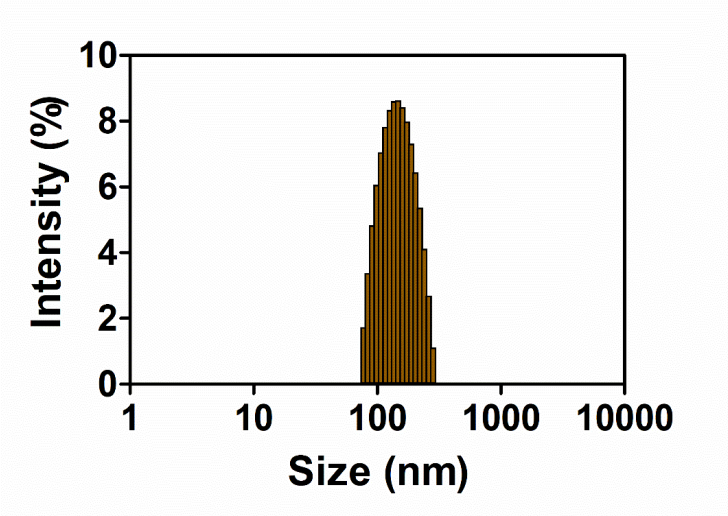

Fig. S24. Hydrodynamic size distribution of NCyNP.

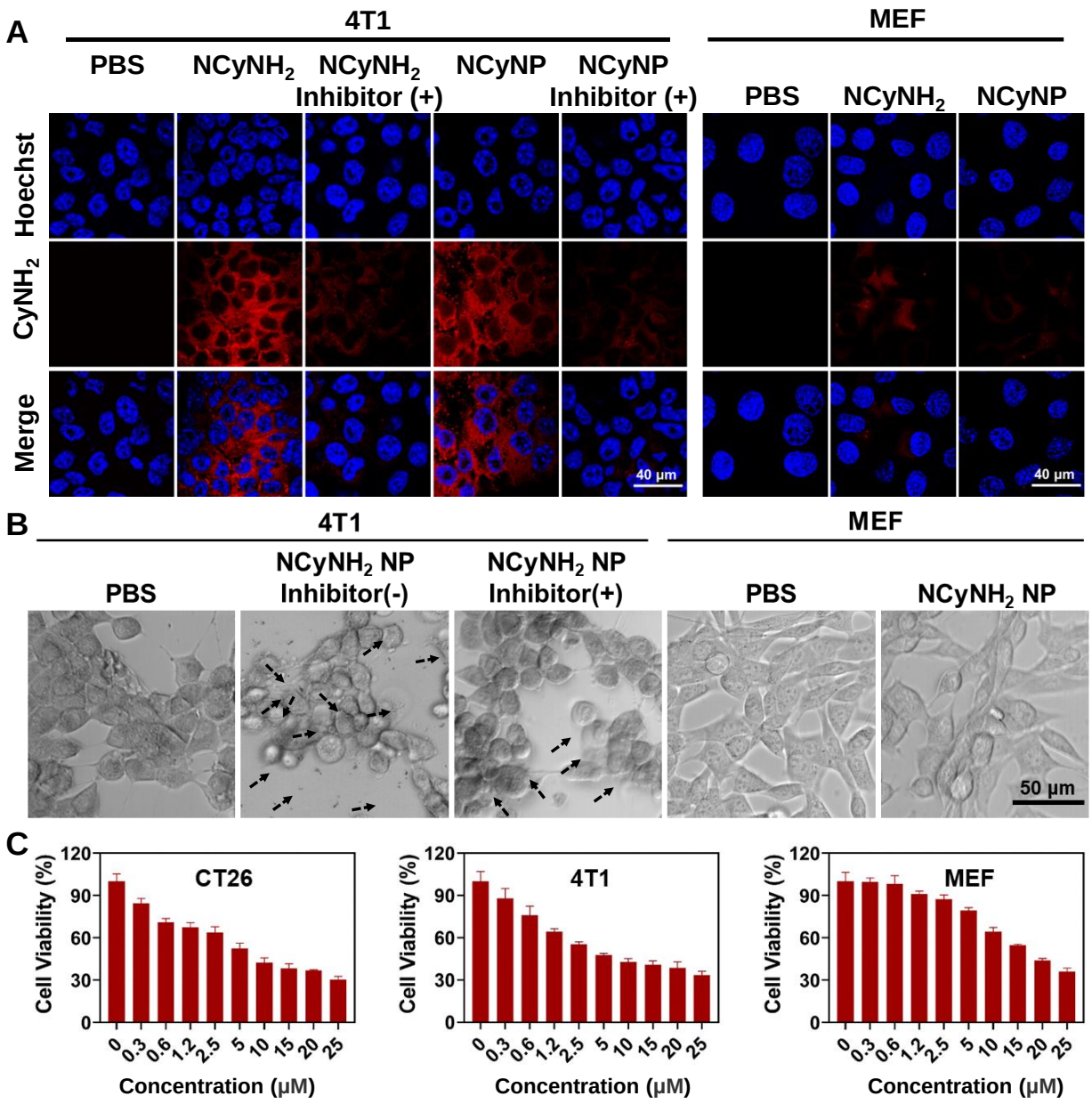

Fig. S25. (A) Confocal images of 4T1 and MEF cells after different treatments. (B) Representative cell morphology of 4T1 and MEF cells after different treatments, the black arrows point to pyroptosis cells. (C) Cell viability of CT26 cells, 4T1 cells and MEF cells treated with different concentrations of NCyNP.

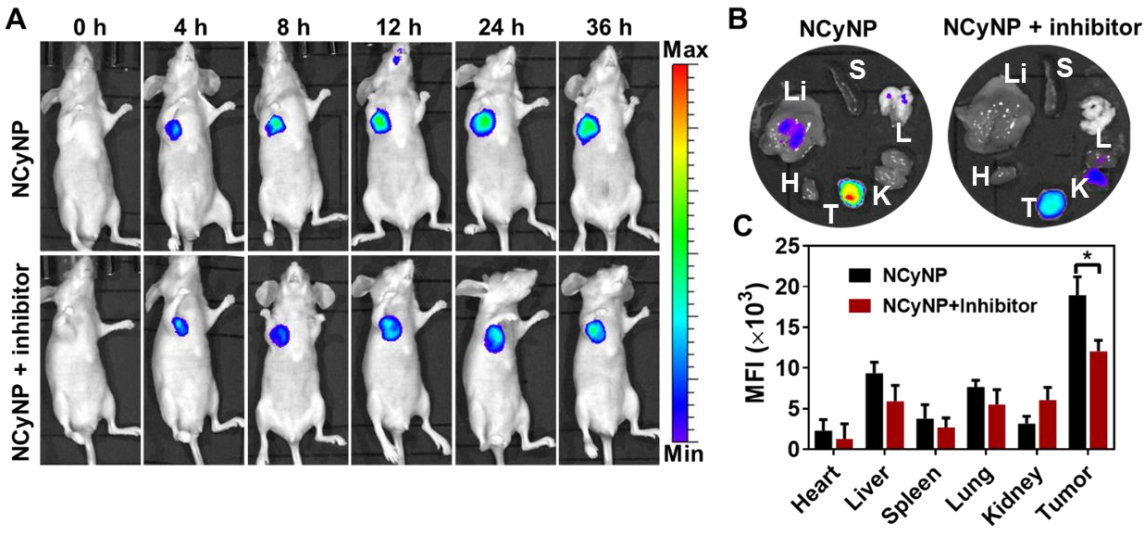

Fig. S26. (A) *In vivo* NIR fluorescence images of nude mice bearing 4T1 tumors after intravenous injection with NCyNP in the absence or presence of NQO1 inhibitor (200 μM, 100 μL dicoumarol, 1 h pretreatment). (B) *Ex vivo* fluorescence imaging of isolated organs (Herat (H), Liver (Li), Spleen (S), Lung (L), Kidney (K)) and tumors (T) collected from mice bearing 4T1 tumors at 36 h after intravenous injection with NCyNP. (C) Quantitative analysis of isolated organ and tumor fluorescence intensity (n = 3). Data are presented as the mean ± SD. Statistical analysis was performed using the Student's t test (ns, nonsignificant. **P* < 0.05, ***P* < 0.01, and ****P* < 0.001).

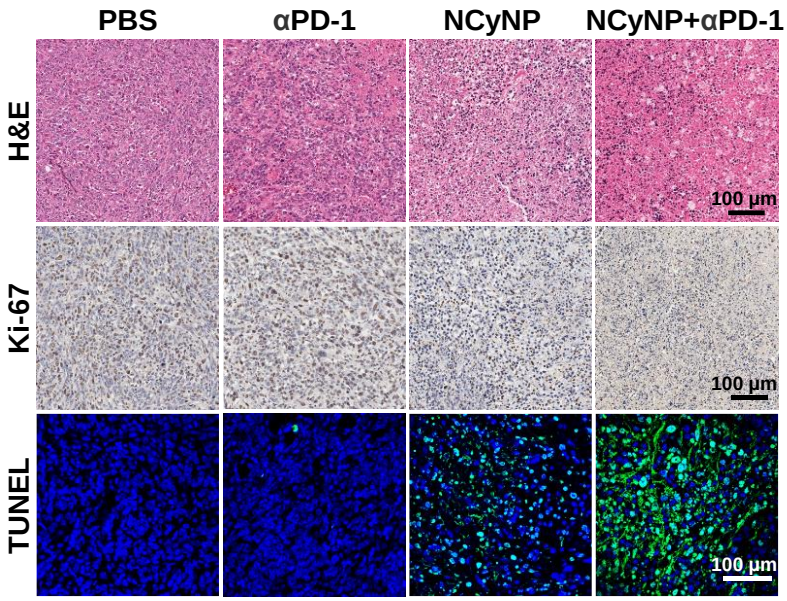

Fig. S27. H&E, Ki-67 and TUNEL staining of tumor tissues after different treatments.

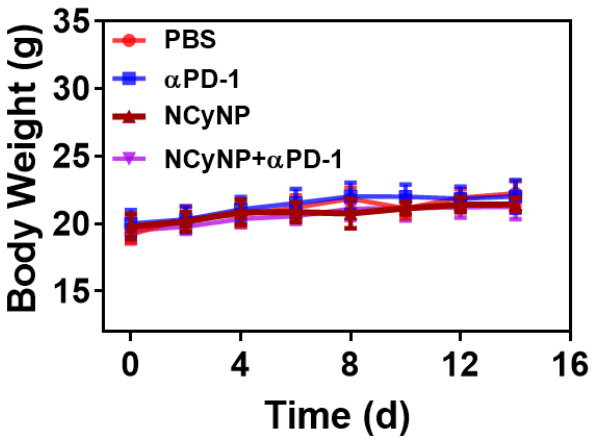

Fig. S28. The body weight change during the treatments.

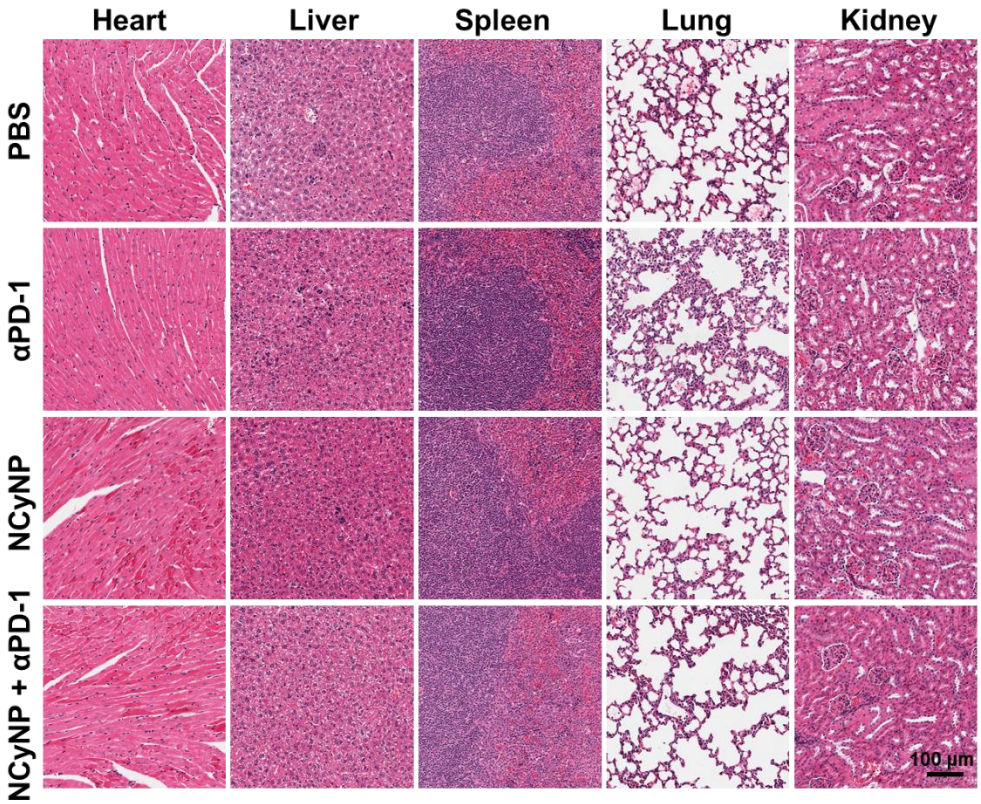

Fig. S29. H&E analysis of main organs after different treatments.

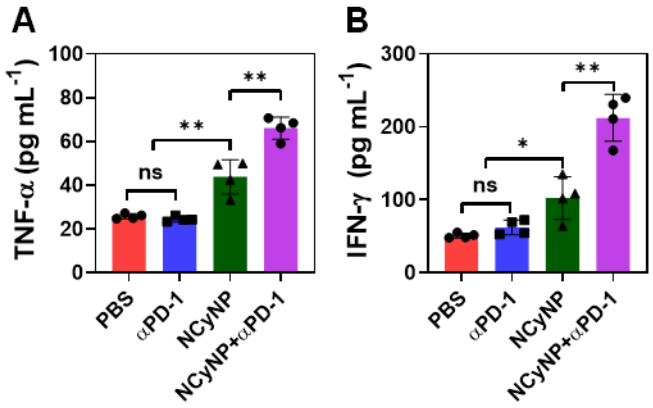

Fig. S30. IFN-γ (A) and TNF-α (B) levels in serum after different treatments. Data are presented as the mean ± SD. Statistical analysis was performed using the Student's t test (ns, nonsignificant. **P* < 0.05, ***P* < 0.01, and ****P* < 0.001).

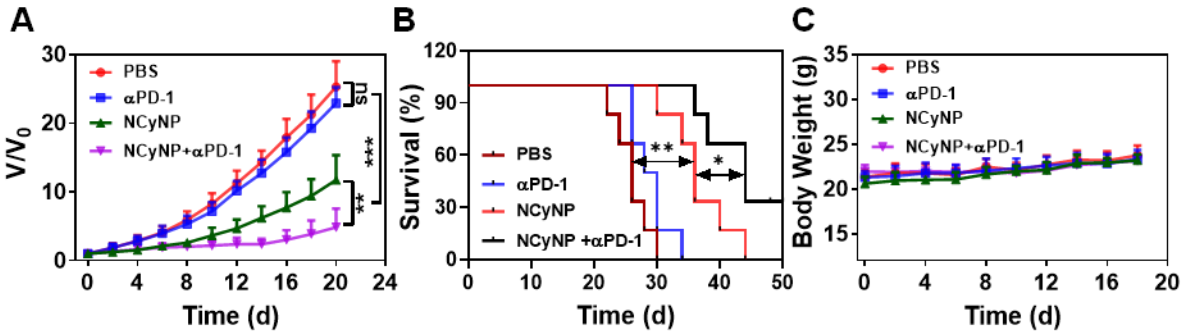

Fig. S31. (A) Tumor growth curves after treatments with PBS, αPD-1, NCyNP, or NCyNP plus αPD-1. (B) Survival rate of mice after treatments with PBS, αPD-1, NCyNP, or NCyNP plus αPD-1. (C) The body weight change during the treatments. Data are presented as the mean ± SD. Statistical analysis was performed using the Student's t test (ns, nonsignificant. **P* < 0.05, ***P* < 0.01, and ****P* < 0.001).

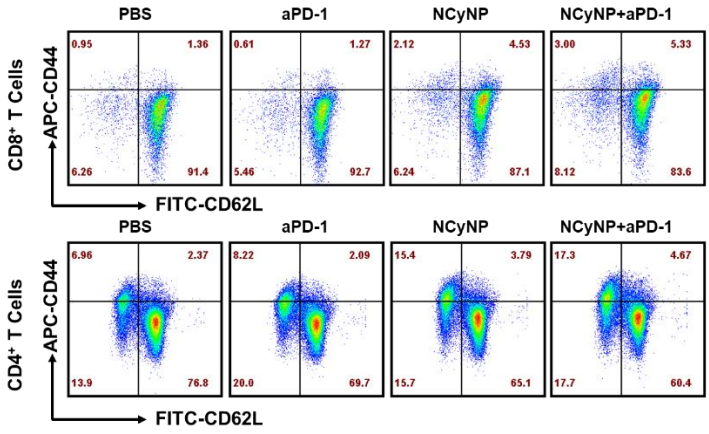

Fig. S32. The representative flow cytometric analysis of $CD8^+$ (or $CD4^+$) central memory T cells ($CD44^{hi}CD62L^{hi}$) and effector memory T cells ($CD44^{hi}CD62L^{low}$) in spleen.